Energy for Sustainable Development 41 (2017) 139–148

Contents lists available at ScienceDirect

Energy for Sustainable Development

A new nozzle design methodology for high efficiency crossflow hydro turbines

R.C. Adhikari, D.H. Wood*

Department of Mechanical and Manufacturing Engineering, University of Calgary, Calgary T2N 1N4, Alberta, Canada

ARTICLE INFO

Article history:
Received 8 March 2017
Received in revised form 30 August 2017
Accepted 8 September 2017

Keywords:
Crossflow turbine
Efficiency
Nozzle
Analytical model
RANS simulation

ABSTRACT

Small-scale hydropower systems are mainly used in remote locations for generating electricity where reasonable hydropower resources are available. Many small-scale systems employ crossflow turbines due to their simplicity in design and manufacture, low cost, sturdy construction and longer life-span. However, compared to most advanced and efficient designs, such as Pelton and Francis turbines, they suffer from a lower maximum efficiency. In a crossflow turbine, the nozzle increases the velocity of the flow and directs it at a suitable angle to the runner whose axis is tangential to the flow. The runner extracts the angular momentum of the flow. Therefore, the runner entry flow is critical for the turbine efficiency. However, it is not yet known clearly how the entry flow affects the runner performance and how the best nozzle can be designed. This study presents a new nozzle design method so that high efficiency crossflow turbines can be designed. An analytical model is formulated to convert the head into kinetic energy at the entry and obtain a suitable flow angle. Three-dimensional Reynolds-Averaged Navier-Stokes simulations were conducted on a 7 kW turbine with a measured maximum efficiency of 69% and a 0.53 kW turbine with a maximum efficiency of 88%. The predictive capability of the computational model was assessed by comparing the computational and experimental results for the power over a range of operating conditions on both turbines. By redesigning only the nozzle of the 7 kW turbine by the new method, the maximum efficiency increased from 69% to 87%. Thus the nozzle design has a significant influence on turbine performance, and we conclude that the conversion of head into kinetic energy and matching of the nozzle flow with the runner design are fundamental in turbine design.

Introduction

Small-scale hydropower systems with the capacity ranging from a few kWs to a few hundred kWs are commonly used in remote communities of the developing countries, especially in those areas where grid extension is too expensive. The primary obstacles to the further adoption of such systems are cost and long-term sustainability. Many small hydropower systems employ crossflow turbines, for example in Nepal where they are also manufactured. These turbines are extremely simple to design and manufacture locally at low cost but suffer from lower efficiency. The current turbine designs have about 70–85% efficiency (Choi et al., 2008; Sinagra et al., 2014; Acharya et al., 2015; Sammartano et al., 2016), whereas the most efficient turbine designs, such as Francis and Pelton, can easily achieve 90% efficiency (Dixon and Hall, 2013; Elbatran et al., 2015). With the current trends towards more efficient turbine designs, simplicity in design and manufacturing and low cost, improvements in their maximum efficiency would lower the cost and improve overall sustainability. In this paper, we present a new nozzle design methodology for improving the maximum efficiency of crossflow turbines. A systematic study was conducted using a two-dimensional (2-D) analytical model for the nozzle design and three-dimensional RANS simulations for evaluating the turbine performance.

The crossflow turbine was invented by Michell (1904) and improved by Banki during 1916–1918, (Desai, 1993). It comprises two main components, a stationary nozzle and a rotating runner, as shown in Fig. 1. The nozzle accelerates the inlet flow and directs it to the runner at a suitable angle, β_1, and so directly affects the runner performance. However, the significance of converting the head into kinetic energy within the nozzle has not been recognized in the past, and there is no design principle for the nozzle as there is for the jet(s) of a Pelton turbine.

As shown in Fig. 1, a unique feature of the crossflow turbine is that flow passes twice through the rotating runner. The flow enters the so-called the first stage, and then traverses through the central

* Corresponding author.
E-mail address: dhwood@ucalgary.ca (D. Wood).

https://doi.org/10.1016/j.esd.2017.09.004
0973-0826/

Nomenclature

H	Turbine head (m)
h_0	Nozzle throat (m)
N	Runner speed (rpm)
N_b	Number of blades
Q	Turbine flow rate (lps)
$R(\theta)$	Radius of nozzle rear-wall
R_1	Outer radius of the runner (m)
R_2	Inner radius of the runner (m)
t	Blade thickness (mm)
u_0	Nozzle inlet velocity (m/s)
u_t	Total velocity (m/s)
u_r	Radial velocity (m/s)
W	Nozzle and runner width (m)
$\dot{W}$	Turbine power (kW)
ω	Runner angular speed (m/s)
β_1	Runner entry flow angle (rad or degrees)
β_{1b}	Outer blade angle (rad or degrees)
β_2	Runner exit flow angle at first stage (rad or degrees)
β_{2b}	Inner blade angle (rad or degrees)
θ_s	Entry arc (rad or degrees)
η	Turbine efficiency (%)

air-space region, and exits through the second stage. Often the first stage does not convert all the available energy into power, (Choi et al., 2008) . Since the outer blade angle, β_{1b}, is likely to be close to β_1, only the blade inner angle, β_{2b}, can be chosen to maximize the second stage performance. These matters will be addressed in a subsequent paper on runner design. Obviously, the double use of the blades presents a challenge to conventional blade terminology: we have used "outer" and "inner" to delineate the blade angles and will continue to do so. In addition, "inlet" describes the flow anywhere in the nozzle with "entry" referring specifically to the flow as it passes from the inlet to the runner.

The majority of previous studies have focused on measurements of turbine performance by varying the runner design parameters

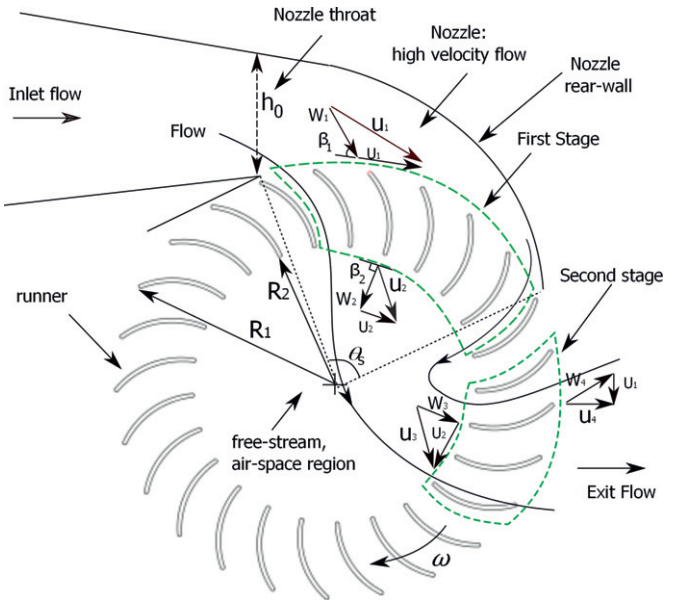

Fig. 1. Schematic illustration of the basic design features of a crossflow turbine.

in attempts to improve the maximum efficiency (Macmore and Merryfield, 1949; Durali, 1976; Nakase et al., 1982; Dakers and Martin, 1982; Khosrowpanah, 1984; Khosrowpanah et al., 1988; Fiuzat and Akerkar, 1989; Desai, 1993; Totapally and Aziz, 1994). However, these studies were primarily single-parameter studies, mainly of the runner, on efficiency. Thus the geometrical parameters for the runner design are well known, but their combined effect on maximum efficiency is not yet clearly understood. Most of these studies reported a maximum efficiency, η_{max}, of less than 82%, which is significantly lower than the typical $\eta_{max} = 90\%$ for the Pelton, Francis and Kaplan turbines. There are only three studies that have reported the η_{max} in the range 88–90% (Fiuzat and Akerkar, 1989; Desai, 1993; Totapally and Aziz, 1994). Based on a limited experimental study, Fiuzat and Akerkar (1989) found $\eta_{max} = 91\%$ when an interior guide tube was used to ensure the water exited through the second stage. However, this maximum efficiency did not occur at maximum flow rate and the paper contains insufficient information on the turbine geometry to allow computational modeling. The turbine power output was not reported. Desai (1993) developed a turbine of power, $\dot{W} = 0.53kW$ with $\eta_{max} = 88\%$ by extensively testing various designs. In continuation of this work, Totapally and Aziz (1994) achieved $\eta_{max} = 90\%$ just by increasing the number of blades, N_b, from 30 to 35. These turbines are the most efficient crossflow turbines reported in the literature and no larger turbines of comparable efficiency have been reported. Fortunately, the references Desai (1993) and Totapally and Aziz (1994) also give sufficient information about the turbine geometry, operating conditions and test results for the turbine efficiency to allow computational simulations and validation, and so this test case is one of the two used in this study. This turbine will be described in the Computational methodology section.

The main nozzle design parameters are the nozzle width, throat h_0, rear-wall shape, $R(\theta) = R_1 + h(\theta)$, where R_1 is the runner outer radius, and entry arc angle, θ_s, as depicted in Fig. 1. The influence of nozzle rear-wall shape was studied by Nakase et al. (1982). They found that both a circular and logarithmic spiral rear-wall gave the same η_{max}. Nakase et al. (1982), Khosrowpanah (1984), and Fiuzat and Akerkar (1989) found that $\theta_s = 90^\circ$ gave the maximum efficiency. Fiuzat and Akerkar (1989) and Totapally and Aziz (1994) similarly found that $\theta_s = 90^\circ$ would improve η_{max} to about 90%. The influence of nozzle design and operating conditions (head and flow rate) was studied by Dakers and Martin (1982). Their 7 kW runner had $\beta_{1b} = 30^\circ$, and $\beta_{2b} = 90^\circ$, the inner to outer radius ratio $R_2/R_1 = 0.68$ and $N_b = 20$ for $H = 10$ m and $Q = 105$ lps. By changing the nozzle configurations, e.g. rear-wall shape and orientation of the nozzle, and keeping the same runner design, they achieved a maximum efficiency of 69%. Their work also gives sufficient information of the turbine geometry, the operating conditions, and test results to allow a detailed computational simulation, and thus it serves as second test case used in this study, which will be described in the Computational methodology section.

No measurements have been reported on the velocity distribution in the inlet flow, velocities and flow angles at the runner entry, and their influence on efficiency. In other words, the only experimental information available is measurements of turbine efficiency as a function of runner speed for different combinations of Q and H. Similarly, the numerical studies were focused mainly on performance prediction of specific turbine designs, rather than on the detailed investigation of the nozzle flow, which is crucial for understanding the design problem and improving the efficiency.

Recent computational studies include Choi et al. (2008), De Andrade et al. (2011), Sammartano et al. (2013), Sinagra et al. (2014), Acharya et al. (2015), and Sammartano et al. (2016), however, these studies contain very little description of the flow and the methods to improve η. This is the key step in addressing the design problem. The previous studies used steady Reynolds-Averaged Navier-Stokes

(RANS) computations employing $k-\epsilon$ and shear stress transport (SST) $k-\omega$ turbulence models combined with homogeneous, two-phase free-surface models for water and air. Moreover, these studies were conducted on low-efficiency turbines, and were primarily aimed at validating the turbine performance measured from experiments. A typical maximum relative error of 10% between the computational fluid dynamics (CFD) and experimental results has been reported by De Andrade et al. (2011). None of these studies addresses the need to convert the head into kinetic energy before the runner entry.

We do not consider a guide vane as used in most actual turbines for controlling the inlet flow. Choi et al. (2008) studied the influence of varying the guide vane angles on turbine efficiency, but they achieved less than 80% efficiency. We anticipate that a guide vane significantly reduces the quality of the inlet flow by splitting it into two jets and producing non-uniform entry flow angles. We will report in a separate study an alternative method of part-load control that maintains high efficiency when combined with the nozzle design method presented in this study.

The remainder of this paper is organized as follows. New nozzle design section presents the new nozzle design methodology, Computational methodology section describes the computational simulations by which we analyze existing nozzle and runner design to establish the accuracy and then analyze the impact of the new nozzle design methodology. Results and discussion section presents the results of the computational studies in which important flow features are characterized followed by the results of design improvements of both turbines and finally, Conclusions section summarizes the findings.

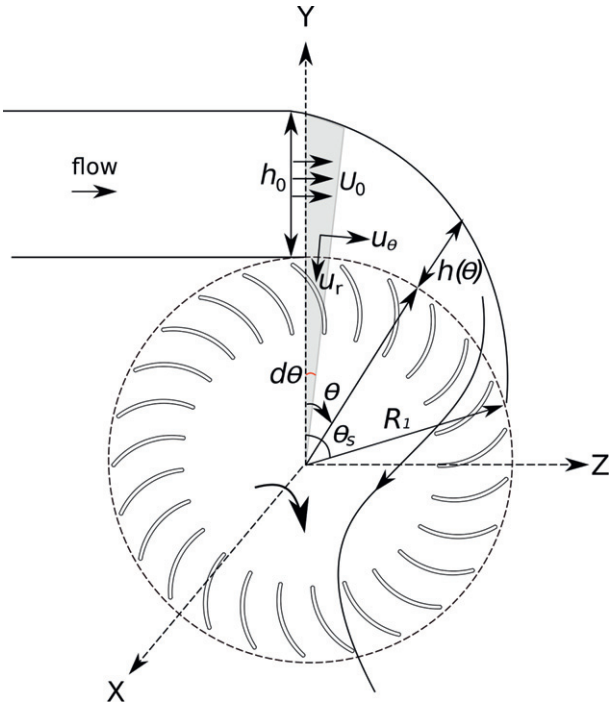

Fig. 2. Schematic illustration of the nozzle configuration with tangential entry in the runner.

New nozzle design

The aim is to determine optimum nozzle dimensions using analytical equations that relate the nozzle throat h_0, the entry arc angle θ_s and the rear-wall shape $R(\theta) = R_1 + h(\theta)$. Since the runner operates under atmospheric pressure, it is assumed that H must be converted into kinetic energy at runner entry to extract maximum power from the flow, which is similar to the design principle for the jets of Pelton turbines, which can exceed 90% efficiency.

It is also assumed that there are negligible viscous losses in the nozzle, and as it is converging, there will be no flow separation from the walls and the boundary layers are likely to decrease in thickness with distance along the nozzle. Bernoulli's equation can be used with reasonable accuracy to calculate nozzle dimensions. The analysis uses the radial and tangential velocity components (u_r and u_θ respectively) in the cylindrical coordinate system as shown in Fig. 2. Initially, the nozzle throat h_0 is aligned radially so the inlet flow is tangential with velocity U_0. In addition, uniform u_r and u_θ are assumed at the runner entry which simplifies the nozzle analysis and ensures that the flow angle will be uniform over the whole entry arc of the runner. Further, the flow is treated as two-dimensional with no variation out of the page in Figs. 1 and 2. The constant nozzle width in that direction, W, is also the width of the runner.

It is also assumed that u_θ is uniform in the nozzle and equal to the velocity at the nozzle throat, i.e. $u_\theta \approx U_0$. Consider a small angle $d\theta$ of the nozzle shown in Fig. 2; continuity applied to the radial and tangential directions using the requirement that u_r is independent of θ gives

$$ru_r d\theta = -h(\theta + d\theta)u_\theta(\theta + d\theta) + h(\theta)u_\theta(\theta) \tag{1}$$

which can be written as

$$ru_r = -u_\theta dh/d\theta. \tag{2}$$

Integration of Eq. (2) gives

$$u_r R_1 \theta = -h(\theta)u_\theta + h_0 U_0. \tag{3}$$

When applied at θ_s, Eq. (3) results in an equation for u_r:

$$u_r = h_0 U_0/(R_1\theta_s). \tag{4}$$

Thus Eq. (3) reduces to

$$h(\theta) = h_0(1 - \theta/\theta_s) \tag{5}$$

and $R(\theta)$ is given by

$$R(\theta) = R_1 + h_0(1 - \theta/\theta_s) \tag{6}$$

This is the equation for tangential entry of the nozzle[1]. The generalized equation for $R(\theta)$ with an arbitrary nozzle orientation shown in Fig. 3 is

$$h(\theta_0+\gamma+\theta) = \left(\sqrt{(R_1\sin\theta_0 + h_0)^2 + (R_1\cos\theta_0)^2} - R_1\right)\left(1 - \frac{\theta}{\theta_s - \gamma}\right) \tag{7}$$

where θ_0 = orientation angle of the left nozzle lip and γ is defined in the Figure. For brevity, the derivation is omitted here; it can be found in Adhikari (2016). This equation allows the design of a nozzle with arbitrary orientation, and will be used in this study for analyzing

[1] A curve of the form of Eq. (6) is called a "neoid" see http://mathworld.wolfram.com/Neoid.html (accessed 21 April 2017).

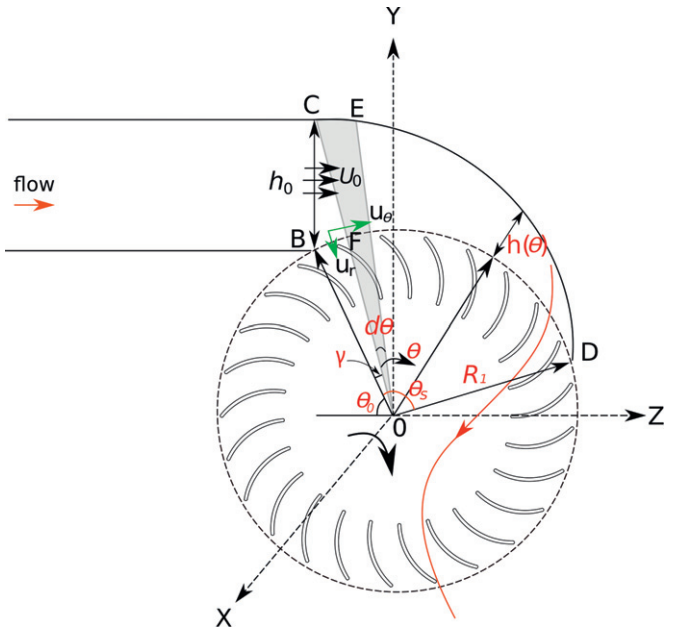

Fig. 3. Schematic illustration of the nozzle configuration with arbitrary orientation.

the nozzles of both the 0.53 kW and 7 kW turbines mentioned in the previous section. It is noted that for tangential entry nozzle, $\theta_0 = 90^\circ$ and $\gamma = 0^\circ$, so Eq. (7) reduces to Eq. (6).

H is converted into kinetic energy when the gauge pressure at runner entry is zero. Thus

$$gH = \frac{1}{2}\left(u_\theta^2 + u_r^2\right) \tag{8}$$

For tangential entry, continuity at the nozzle throat h_0 and Eq. (4) gives

$$gH = \frac{U_0^2}{2}\left(1 + \frac{h_0^2}{R_1^2\theta_s^2}\right) \tag{9}$$

and

$$\beta_1 = \tan^{-1}\left(\frac{u_r}{u_\theta - \omega R_1}\right) \tag{10}$$

where ω is the angular velocity of the runner. Good turbine design requires that $\beta_1 \sim \beta_{1b}$ to avoid flow separation. Thus the conditions that give the best nozzle performance also give essential information for the runner design.

The angular momentum flux at the runner entry is

$$\rho W R_1^2 u_\theta u_r \theta_s = \rho W R_1 U_0 h_0 U_0 \tag{11}$$

If we assume that all power is extracted by the first stage the runner shaft power $\dot{W}$ is

$$\dot{W} = \rho Q U_0 R_1 \omega. \tag{12}$$

Combining this with the energy equation:

$$\rho Q U_0 R_1 \omega = \rho Q g H \tag{13}$$

gives the condition for optimal runner speed, ω_{max}:

$$\frac{\omega_{max} R_1}{U_0} = \frac{1}{2}\left(1 + \frac{h_0^2}{R_1^2\theta_s^2}\right) \tag{14}$$

Eq. (14) shows that η_{max} occurs at around a tip-speed ratio of 0.5 as typically, $h_0^2/(R_1^2\theta_s^2)$ is significantly less than unity. It is noted that this is the same tip speed ratio for optimizing the Pelton turbine when losses in the jet and elsewhere are ignored. Eq. (14) shows that there is only one ω and Q for which the head H can be fully converted into kinetic energy to obtain the maximum efficiency. From the point of view of control, this is highly important because flow control must be used for part-load operation, that is reduced Q at the same H, and it is not possible to rely on electronic control of the generator to maintain high efficiency.

Computational methodology

Large eddy simulations (LES) or direct numerical simulations (DNS) of the Navier-Stokes equations are still too computationally expensive to be feasible for analyzing turbomachinery with multiphase flows such as in crossflow turbines. This work used common steady and unsteady RANS models to reduce the cost of the simulations and two-phase homogeneous flow with free-surface effects was assumed. The SST $k-\omega$ turbulence model provided satisfactory results for the turbine performance compared to the $k-\omega$ and $k-\epsilon$ models. Previous studies have reported satisfactory prediction of crossflow turbine efficiency with this computational model (Choi et al., 2008; De Andrade et al., 2011; Sammartano et al., 2013; Sinagra et al., 2014; Acharya et al., 2015; Sammartano et al., 2016).

Modeled turbines

Two turbine models were chosen for the computational analysis. The first produced 7 kW with $\eta_{max} = 69\%$, Dakers and Martin (1982). The second, 0.53 kW turbine achieved $\eta_{max} = 88\%$, Desai (1993). The important geometrical features of these turbines are shown in Figs. 4 and 5 respectively, and the corresponding geometrical parameters are presented in Table 1. In both cases, the turbine performance was measured over a wide range of operating conditions. However, the flow characteristics and the causes of losses are not known for either turbine.

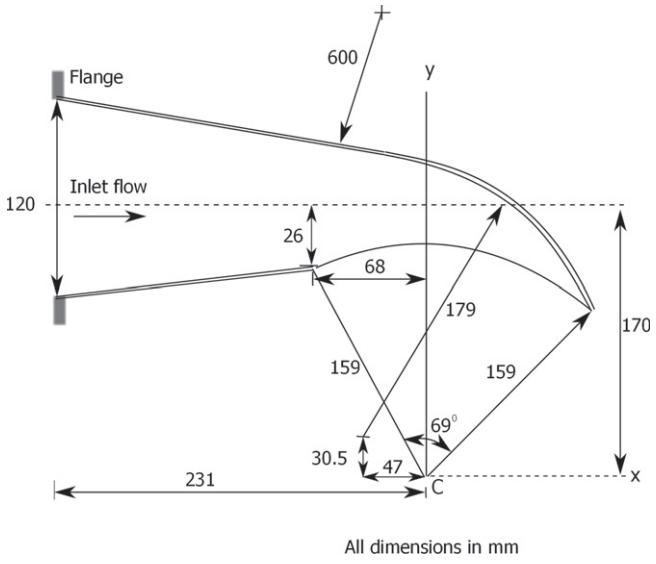

Fig. 4. Schematic illustration of the nozzle of 7 kW turbine with $\eta_{max} = 69\%$.

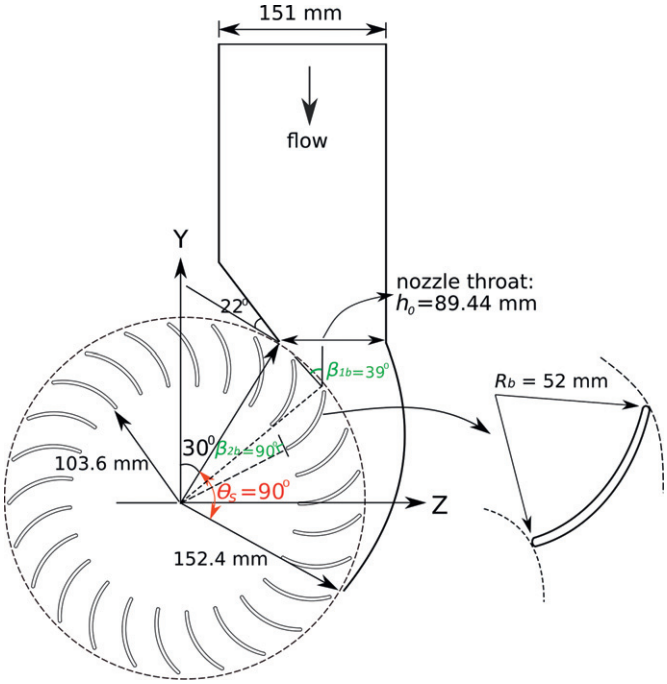

Fig. 5. Schematic illustration of the 0.53 kW turbine with $\eta_{max} = 88\%$.

Computational model

The flow in crossflow turbines consists of water and air, and is characterized by free-surface effects. The flow was assumed homogeneous with free-surface effects between the water and air. In a homogeneous multiphase flow, each fluid may possess its own flow field or all fluids may share a common flow field. The fluids are mixed only at the macroscopic scale with a discernible interface between them, Brennen (2005), ANSYS (2016). In this model, air and water are assumed to share the same pressure and velocity fields as well as the turbulence fields. In a free-surface flow of water and air, there is a thin interface between water and air. The free-surface model attempts to resolve the interface between the two. In a homogeneous multiphase flow, RANS equations are solved for both fluids. We performed steady and unsteady RANS simulations with the SST $k-\omega$ turbulence model as did Adhikari et al. (2016). The standard values of the model constants were not modified from those given in ANSYS (2016). For brevity, we omit the details of the mathematical descriptions of the models as they can be found in Adhikari (2016). We note that the inlet and runner entry flows were entirely water, in other words, were single phase. The multiphase model is needed primarily for the second stage and runner exit flow.

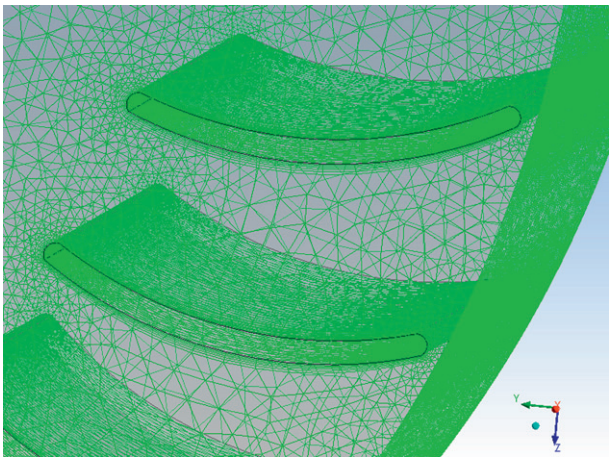

Fig. 6. A zoomed view of the mesh resolution around the blades.

Computational mesh

An unstructured tetrahedral mesh with hexahedral elements with prismatic layers in the near wall region. A typical computational mesh used in the simulation is shown in Fig. 6. The computational domain was divided into two sub-domains: stationary (nozzle) and rotating (runner). A general grid interface (GGI) connected the two domains, which allows updating on interface position at each time step while the relative position of the grids on each side of the interface change due to runner rotation (ANSYS, 2016) . The GGI also allows non-matching grid points to communicate with each other via interpolation (ANSYS, 2016) .

A grid convergence study was carried out by gradually refining the mesh size starting from 2.1 million elements until an acceptable convergence was achieved for $\dot{W}$. Mesh resolution was systematically assessed by computing the value of y^+, the non-dimensional distance of the first mesh node from the wall, because SST $k-\omega$ requires $y^+ < 5$, (Menter, 1994; ANSYS, 2016) for high accuracy. A total of 5.4 million elements were required to produce grid independent $\dot{W}$ for the 7 kW turbine, which corresponds to less than 0.1% uncertainty in the computed results due to grid resolution (Oberkampf and Trucano, 2000; Roache, 1997) . Similarly, about 14 million elements were required for the 0.53 kW turbine to produce mesh independent results. The results of the mesh independent study for the 7 kW turbine is reported in Table 2.

Boundary conditions

The inlet and outlet boundary conditions correspond to the experimentally tested values for H and Q at different runner speeds N. At the inlet, total pressure corresponding to the operating head H was specified with a turbulence intensity of 5%. The outlet mass

Table 1
Design parameters of 7 kW and 0.53 kW turbines.

Design parameter	7 kW turbine	0.53 kW turbine
Outer radius (R_1), [mm]	158	76.2
Inner radius (R_2), [mm]	105.86	51.8
Outer blade angle (β_{1b}), [deg]	30	39
Inner blade angle (β_{2b}), [deg]	90	90
Blade thickness (t), [mm]	3	3.2
Number of blades (N_b)	20	30
Runner and nozzle width (W), [mm]	150	101.6
Nozzle throat (h_0), [mm]	65	89
Nozzle entry arc (θ_s), [deg]	69	90

Table 2
Summary of mesh independence test.

Mesh	No of elements	$\dot{W}$ (kW)	Numerical error (%)
Mesh 1	2.12 million	7.091	-
Mesh 2	2.96 million	7.122	0.43
Mesh 3	3.47 million	7.157	0.49
Mesh 4	3.94 million	7.169	0.16
Mesh 5	4.53 million	7.181	0.16
Mesh 6	5.24 million	7.192	0.15
Mesh 7	5.40 million	7.199	0.10

flow rate was specified. Although not shown here, both turbines had air vents in the casing surrounding the runner. At the vents, the "opening" type boundary condition was specified. A uniform profile of the inlet flow was assumed at the upstream boundaries of the computational domains shown in Figs. 4 and 5 as no experimental velocity profile was available. The consequence of non-uniformity at the inlet, if any, on the runner performance should be small as the inlet was kept far upstream from the runner.

Results and discussion

First, the CFD and experimental $\dot{W}$ are compared. The main features of the flow fields are then examined and compared to characterize the influence of the inlet flow conditions or the nozzle design on runner performance. Then the new nozzle design was introduced without changing the runners.

Turbine output power

Results from steady and unsteady RANS computations for $\dot{W}$ are shown in Fig. 7 for the 7 kW turbine. There is satisfactory agreement with a relative error of less than 6%. Similarly, the CFD and experimental results for the 0.53 kW turbine disagreed by less than 3.8%, Fig. 8. These results are more accurate than, for example, the 10% relative error reported by De Andrade et al. (2011). In addition, steady and unsteady RANS computations gave very similar results for $\dot{W}$, so only the former are considered here. The unsteady RANS results can be found in Adhikari (2016).

Nozzle flow characteristics

The velocity profile and flow angle at the runner entry of the 7 kW turbine are plotted in Figs. 9 and 10 respectively. Note that, partly for clarity, u_r is properly plotted as a negative quantity rather than as a positive one as assumed in New nozzle design section. The velocities are relative to an observer rotating with the blades, as are all velocities presented in this paper, and the azimuthal angle is the angular position of the nozzle entry arc measured from the horizontal direction in Fig. 4. The large difference between the computed total velocity, $u_t = \left(u_r^2 + u_\theta^2\right)^{1/2}$, and the ideal total entry velocity from Eq. (4) and $u_\theta \sim U_0$, shows that the nozzle does not completely

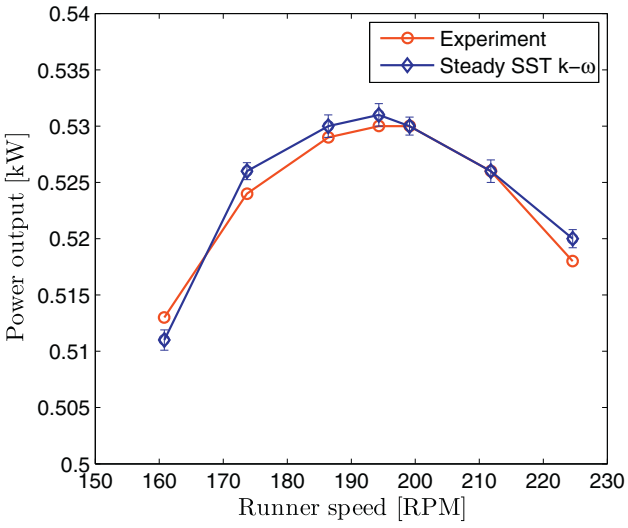

Fig. 8. Comparison of CFD and experimental results for the output of the 0.53 kW turbine at $Q = 46$ lps and $H = 1.33$ m.

convert H into kinetic energy at the runner entry. Eq. (4) is equivalent to $u_r = Q/(R_1\theta_s W)$. Similarly, there is a significant difference between β_1 and β_{1b}, which has resulted in massive flow separation on the first stage blades as shown in Fig. 11. To improve the power extraction in the runner, the differences in angle must be reduced.

For the 0.53 kW turbine with $\eta_{max} = 88\%$, Figs. 12 and 13 show the velocity profile and flow angle at the runner entry. Note that the origin for the azimuthal position is the negative z–direction in Fig. 5. The total velocity at the runner entry is approximately equal to the ideal total velocity. This implies that H is converted into kinetic energy. No details of the nozzle design were given by Desai (1993) so it is unknown whether this conversion was deliberate or a happy accident.

The 0.53 kW turbine shows some differences between β_1 and β_{1b}, but there is no flow separation on the blades, (Fig. 14). However, as in the 7 kW turbine, there are azimuthal variations in u_θ and u_r particularly near the throat. As a result, β_1 has decreased from 75 to about 37° in this section. It is noted that β_1 is comparable to

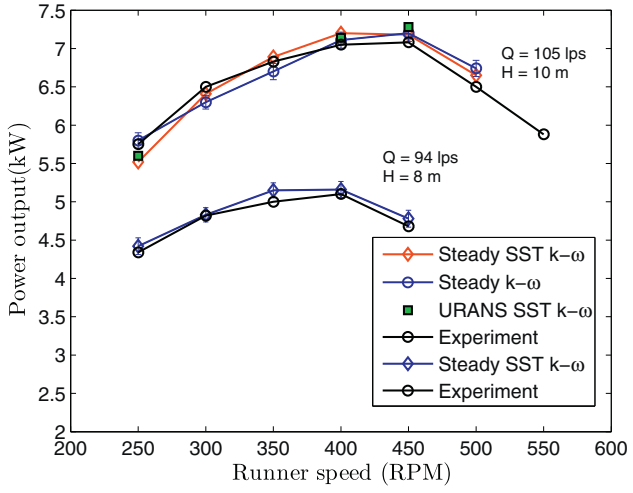

Fig. 7. Comparison of CFD and experimental results for the power output of the 7 kW turbine at different flow rates and heads.

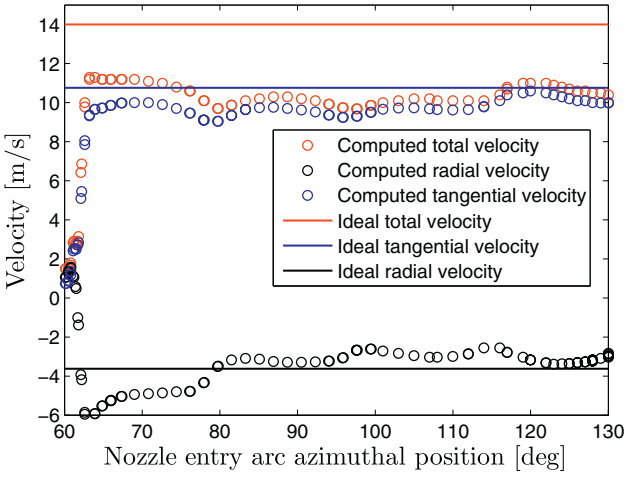

Fig. 9. Ideal and computed total, tangential and radial velocities at the runner entry of the 7 kW turbine at $\eta_{max} = 69\%$, $Q = 105$ lps and $H = 10$ m.

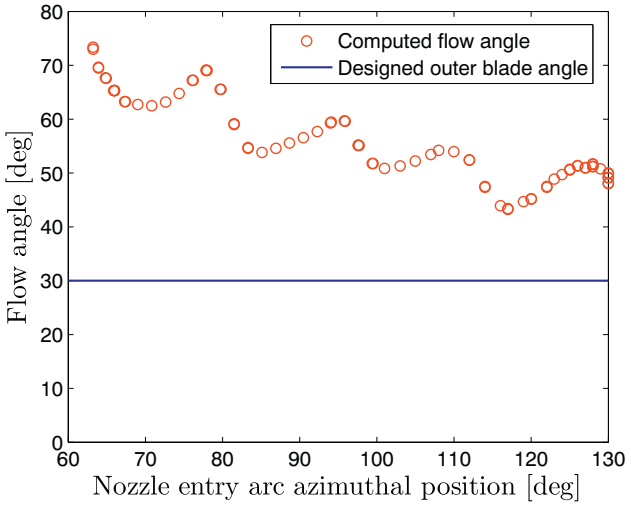

Fig. 10. Comparison of the computed inlet flow angle β_1 with the outer blade angle at the inlet of the runner of the 7 kW turbine at $\eta_{max} = 69\%$, $Q = 105$ lps, $H = 10$ m and $N = 450$ RPM.

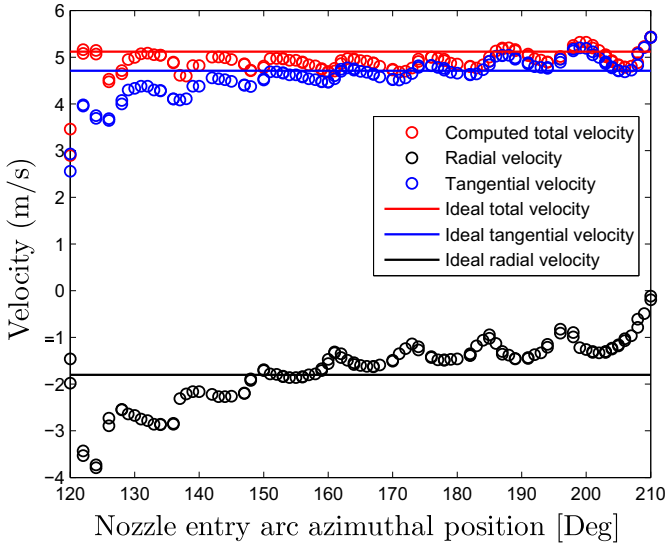

Fig. 12. Ideal and computed total, tangential and radial velocities at the runner entry of the 0.53 kW turbine at $\eta_{max} = 88\%$, $Q = 46$ lps, $H = 1.33$ m and $N = 199.1$ RPM.

β_{1b} ($= 39^\circ$) over a larger extent of the runner inlet. It is remarkable that in the actual design of this turbine by Desai (1993), β_1 was assumed to be azimuthally uniform despite the fact that it has not been explicitly described by the author and the entry flow was not measured. Clearly, the small area of difference between β_1 and β_{1b} and the azimuthal non-uniformity of the angular momentum flux do not cause a significant lowering of efficiency. The main reasons are: 1) H is approximately converted into kinetic energy in any case, 2) power is extracted in two stages, so the energy in the entry flow with high β_1 that is not converted in the first stage can still be captured in the second stage, 3) flow separation was reduced by having a larger number of blades, and 4) close matching between β_1 with β_{1b} over a large extent of the runner inlet.

The failure of the nozzle in the inefficient 7 kW turbine to convert H to kinetic energy in contrast to the 0.53 kW nozzle achieving this conversion, implies the importance of the nozzle design. To investigate this further, the nozzle of the 7 kW turbine was redesigned using the methodology of New nozzle design section. The results are presented in the next section.

Application of the new nozzle design

To improve the performance of the 7 kW turbine, the nozzle was redesigned using the new analytical model, and then computations were performed without altering the original runner design. This allowed identification of the major changes in the runner inlet flow and the runner performance and validation of the new nozzle design methodology.

For the design $Q = 105$ lps and $H = 10$ m, a range of possible values h_0 and nozzle width W are possible, but those used in the original nozzle design did not allow conversion of H into kinetic energy. Therefore, it was decided to use the same $W/h_0 = 1.14$ as the high efficiency 0.53 kW turbine for the redesign of the 7 kW one. For similar reasons, θ_s was increased from 69 to 80°. Then conversion of H into kinetic energy gave $h_0 = 83$ mm and $W = 94.34$ mm which is significantly smaller than for the original design; a reduced W should reduce manufacturing costs as well. The nozzle orientation was kept

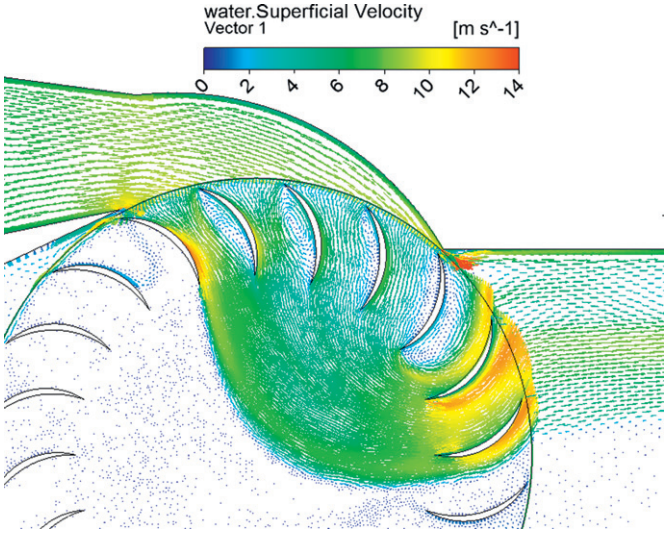

Fig. 11. Water velocity vectors illustrating the flow separation on the blades at the first stage of the 7 kW turbine at $\eta_{max} = 69\%$. Note that there is no flow separation on the second stage.

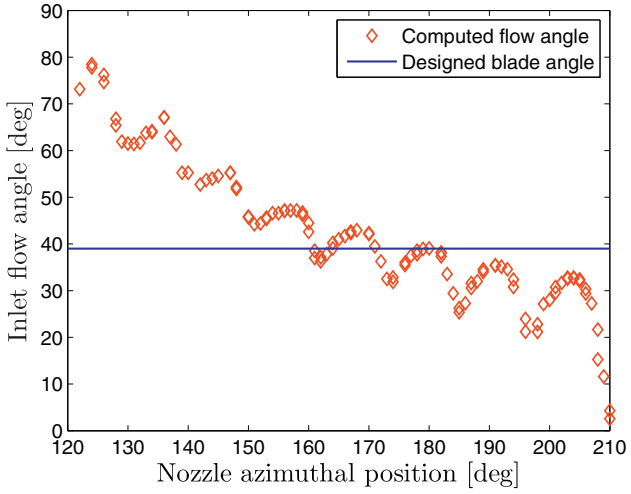

Fig. 13. Azimuthal variation of the inlet flow angle β_1 at the runner inlet of the 0.53 kW turbine at $\eta_{max} = 88\%$, $Q = 46$ lps, $H = 1.33$ m and $N = 199.1$ RPM.

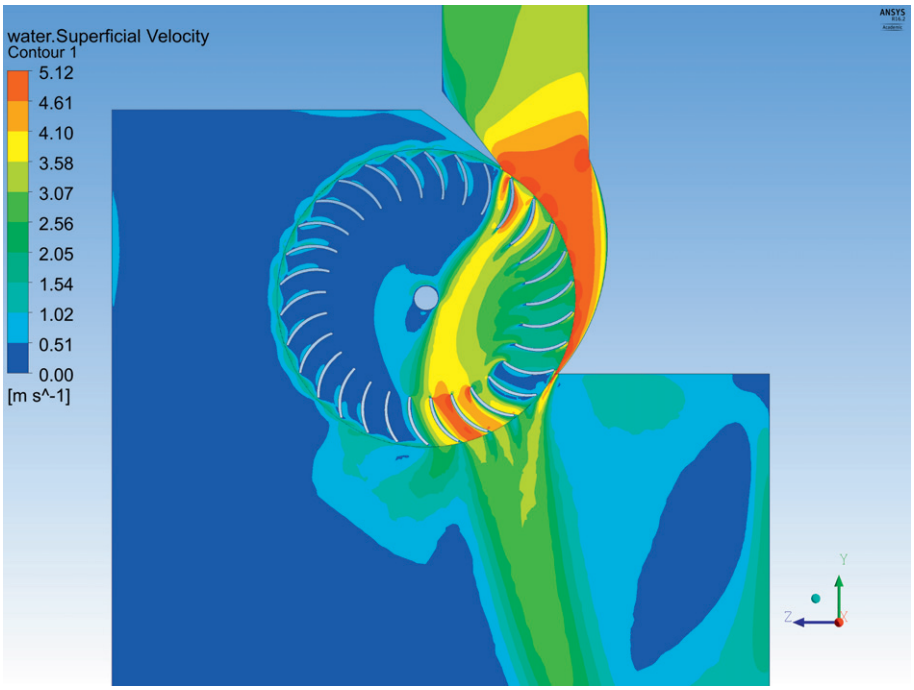

Fig. 14. Contour plot of the magnitude of mean water velocity of the 0.53 kW turbine at η_{max}, $Q = 46$ lps, $H = 1.33$ m and $N = 199.1$ RPM.

the same. A summary of design parameters for the new nozzle is presented in Table 3.

By re-designing the nozzle without altering the runner, η_{max} increased from 69 to 87%. A comparison of the computed total, radial and tangential velocities at the runner entry with the ideal velocities for the new nozzle is shown in Fig. 15 for $Q = 105$ lps, $H = 10$ m, and $N = 500$ RPM. For the new nozzle, the total velocity is approximately equal to the ideal total inlet velocity of 14 m/s, implying that the head H is converted into kinetic energy. This means that the angular momentum flux at the runner inlet has increased compared to the original nozzle. It is observed that the computed total inlet velocity is azimuthally uniform but neither u_r nor u_θ is uniform, which will cause an azimuthal variation of β_1. Eq. (10) gives $\beta_1 = 40^\circ$ and $\eta = \eta_{max}$ at $N = 460$ RPM. A comparison of β_1 and the unchanged $\beta_{1b} = 30^\circ$ for the runner entry from the new nozzle and the original nozzle is shown in Fig. 16. The difference in optimal speed of 500 RPM for the new nozzle compared to 460 RPM, is explained by the fact that β_{1b} has not been reduced from its original value and this will require a higher N to match β_{1b} and β_1. It is noted that there is negligible flow separation in the first stage of the runner compared to the original nozzle as shown in Fig. 17. There is, however, now some separation on the suction sides of the blades at the second stage. The normalized u_θ contours plotted in Fig. 18 illustrate that the new nozzle design method is accurate except at the very right nozzle lip. Contours of u_r in Fig. 19 are not so uniform and generally smaller in magnitude than the simple model. This may reflect the influence of the blades on the inlet flow. It is also interesting to note that the azimuthal variation of β_1 is very similar to that of the high-efficiency 0.53 kW turbine as discussed in the previous section.

Table 3
New nozzle design parameters for the 7 kW turbine.

Design parameter	Value
Nozzle throat: h_0 [mm]	83
Nozzle width: W [mm]	94.34
Nozzle entry arc: θ_s [°]	80
Inclined angle of lower inlet wall: δ [deg]	22

Conclusions

We presented a simple, new analytical model for nozzle design to achieve higher efficiency of crossflow turbines which are commonly used in small-scale hydropower systems around the world. A systematic computational study on the influence of nozzle design on the runner performance has been performed. It was shown that nozzle design plays a significant role in determining turbine efficiency, and a procedure for designing optimum nozzles has been demonstrated through computational simulations. The study

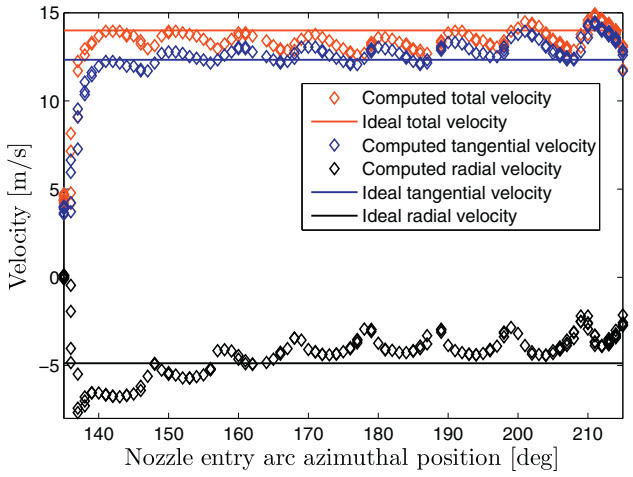

Fig. 15. Comparison of u_r and u_θ with the ideal velocities at the runner entry of the 7 kW turbine with the new nozzle, $Q = 105$ lps, $H = 10$ m and $N = 500$ RPM.

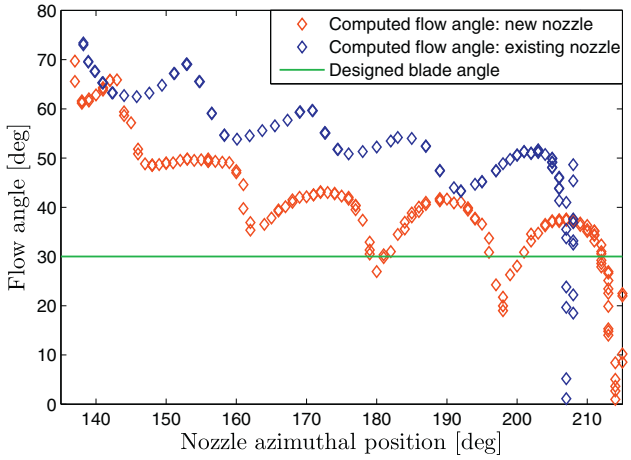

Fig. 16. Comparison of β_1 and β_{1b} at η_{max} for the 7 kW turbine with the new nozzle (500 RPM) and the existing nozzle (450 RPM) at $Q = 105$ lps and $H = 10$ m.

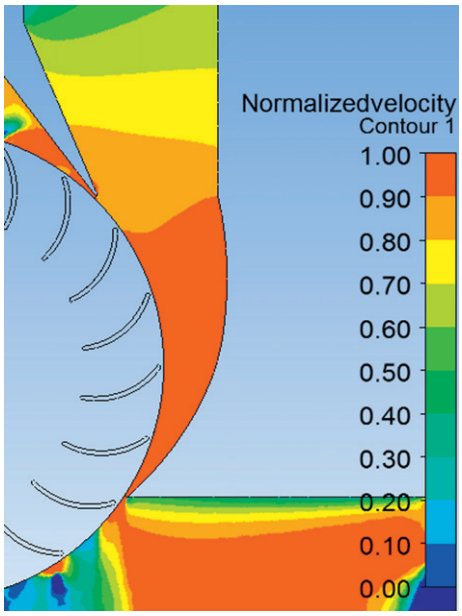

Fig. 18. Normalized tangential velocity u_θ/U_0 contours in the new nozzle at η_{max}. $Q = 105$ lps, $H = 10$ m, and $N = 500$ RPM.

was carried out using three-dimensional Reynolds-Averaged Navier-Stokes simulations with SST $k-\omega$ turbulence model and a two-phase homogeneous free-surface flow model. Two small-scale crossflow turbines, one of 7 kW capacity with a maximum efficiency of 69% and another of 0.53 kW capacity with a maximum efficiency of 88%, were studied as reference turbines for validation, and design improvement was conducted for the 69% efficient turbine. The main conclusions drawn from this study regarding the significance of nozzle design are summarized as follows.

1. A two-dimensional analytical model was formulated for the nozzle design. This model gives equations for determining the rear-wall shape of the nozzle, entry arc and rear-wall shape based on the flow rate and operating head. The equation further gives the condition for converting the head into kinetic energy and inlet flow angle and the optimum operating speed for the runner.

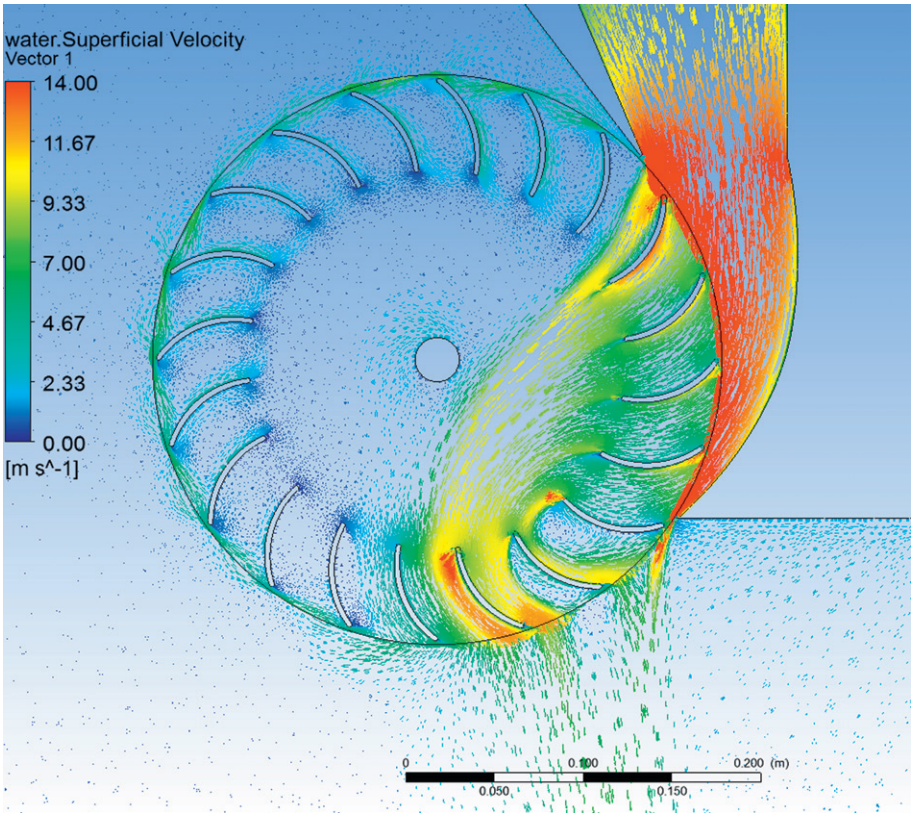

Fig. 17. Water velocity vectors illustrating the reduction in flow separation in the runner of the 7 kW turbine with the new nozzle at η_{max}. $Q = 105$ lps, $H = 10$ m, and $N = 500$ RPM.

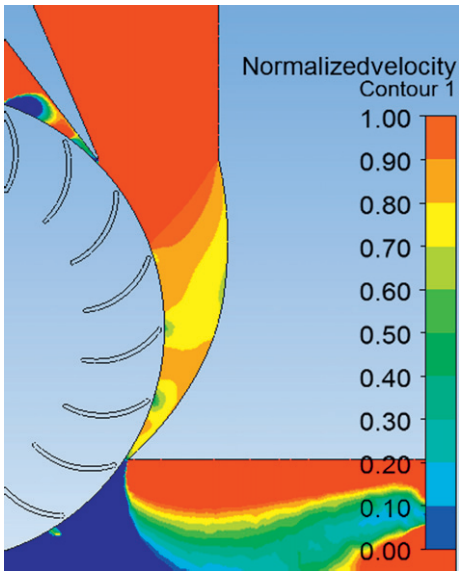

Fig. 19. Normalized radial velocity $u_r/(R_1 U_0 \theta_s)$ contours in the new nozzle at η_{max}. $Q = 105$ lps, $H = 10$ m, and $N = 500$ RPM.

2. The computation of the flow at the runner entry of the 69% efficiency turbine showed that the head was not fully converted into kinetic energy and the inlet flow angle and the outer blade angle at the maximum efficiency did not match, which resulted in massive flow separation and performance loss. In contrast, the nozzle of of 88% efficient turbine converted the head into kinetic energy and the inlet flow angle matched closely the outer blade angle over a large part of the runner entry. This validated the basic principle of the new model that all the head must be converted into kinetic energy and inlet flow angle must closely match the outer blade angle to maximize power extraction. However, it is not clear whether the nozzle was designed using the principle of conversion or whether it was a happy accident.
3. With the new nozzle methodology applied to the 7 kW turbine, the head was converted into kinetic energy and a better match between the inlet flow angle and outer blade angle was achieved, which improved the turbine efficiency from 69% to 87%. Thus the design principle for the nozzle was further validated. In addition, the computational simulations showed the need to have the blade outer angle approximately equal to the flow angle at the runner entry.

The results of this study highlight the significance of nozzle design in crossflow turbines. The analytical model allows the nozzle to match the entry flow with the runner design to achieve maximum efficiency. We anticipate that this work will stimulate further computational studies of the design of crossflow turbines to achieve higher efficiency and, hopefully, flow measurements within the nozzle and runner. Subsequent papers will investigate runner design and a method for maintaining part-load efficiency which fits neatly into the nozzle design process described here.

Acknowledgments

The authors acknowledge the funding support from NSERC/ENMAX Research Chair in Renewable Energy at the University of Calgary, Canada. We would also like to acknowledge WestGrid Canada for providing high-performance computers to perform flow simulations.

References

Acharya N, Kim C-G, Thapa B, Lee Y-H. Numerical analysis and performance enhancement of a cross-flow hydro turbine. Renew Energy 2015;80:819–26.
Adhikari R. Design improvement of crossflow hydro turbine.Ph.D. thesis. Canada: University of Calgary; 2016.
Adhikari RC, Vaz J, Wood D. Cavitation inception in crossflow hydro turbines. Energies 2016;9:237–48.
ANSYS, Ansys Academic research. USA: ANSYS Inc; 2016.
Brennen CE. Fundamentals of multiphase flow. Cambridge University Press.; 2005.
Choi YD, Lim JI, Kim YT, Lee YH. Performance and internal flow characteristics of a cross-flow hydro turbine by the shapes of nozzle and runner blade. J Fluid Sci Technol 2008;3:398–409.
Dakers A, Martin G. Development of a simple cross-flow water turbine for rural use. Agricultural Engineering Conference 1982: Resources, Efficient Use and Conservation; Preprints of Papers. Australia: Institution of Engineers1982. p. 35.
De Andrade J, Curiel C, Kenyery F, Aguillón O, Vásquez A, Asuaje M. Numerical investigation of the internal flow in a Banki turbine. Int J Rotating Mach 2011;2011:1–12.
Desai VR. A parametric study of the cross-flow turbine performance.Ph.D. thesis. USA: Clemson University; 1993.
Dixon SL, Hall C. Fluid mechanics and thermodynamics of turbomachinery. Butterworth-Heinemann.; 2013.
Durali M. Design of small water turbines for farms and small communities.Ph.D. thesis. USA: Massachusetts Institute of Technology; 1976.
Elbatran A, Yaakob O, Ahmed YM, Shabara H. Operation, performance and economic analysis of low head micro-hydropower turbines for rural and remote areas: a review. Renew Sustain Energy Rev 2015;43:40–50.
Fiuzat A, Akerkar B. The use of interior guide tube in cross flow turbines. Waterpower89. American Society of Civil Engineers.1989. p. 1111–9.
Khosrowpanah S. Experimental study of the crossflow turbine.Ph.D. thesis. USA: Colorado State University; 1984.
Khosrowpanah S, Fiuzat A, Albertson ML. Experimental study of crossflow turbine. J Hydraul Eng 1988;114:299–314.
Macmore C, Merryfield F. The Banki water turbine. Eng Exp Stn 1949;25:3–25.
Menter FR. Two-equation eddy-viscosity turbulence models for engineering applications. AIAA J 1994;32:1598–605.
Michell A. Impulse-turbine. Assignee, patent no 760898, United States Patent Office, 1904, 1904.
Nakase Y, Fukutomi J, Watanabe T, Suetsugu T, Kubota T, Kushimoto S. A study of cross-flow turbine (effects of nozzle shape on its performance). Proceedings of the Winter Annual Meeting ASME, Phoenix, AZ, USA. vol. 1419. 1982.
Oberkampf WL, Trucano TG. Validation methodology in computational fluid dynamics. AIAA 2000;2549:19–22.
Roache PJ. Quantification of uncertainty in computational fluid dynamics. Annu Rev Fluid Mech 1997;29:123–60.
Sammartano V, Aricò C, Carravetta A, Fecarotta O, Tucciarelli T. Banki-Michell optimal design by computational fluid dynamics testing and hydrodynamic analysis. Energies 2013;6:2362–85.
Sammartano V, Morreale G, Sinagra M, Tucciarelli T. Numerical and experimental investigation of a cross-flow water turbine. J Hydraul Res 2016;54:321–31.
Sinagra M, Sammartano V, Aricò C, Collura A, Tucciarelli T. Cross-flow turbine design for variable operating conditions. Proc Eng 2014;70:1539–48.
Totapally HG, Aziz NM. Refinement of cross-flow turbine design parameters. J Energy Eng 1994;120:133–47.